Transmission through Single and Multiple Layers in the 3-10 GHz Band and the Implications for Communications of Frequency Varying Material Dielectric Constants

A. YAHALOM, Y. PINHASI, E. SHIFMAN AND S. PETNEV

Department of Electrical & Electronic Engineering, Faculty of Engineering,
Ariel University Center of Samaria
Kiryat Hamada, P.O.B. 3, Ariel 40700
ISRAEL
asya@ariel.ac.il http://www.ariel.ac.il/sites/ayahalom/

Abstract: - In this work we describe a model taking into account transmission through single and multiple layers which are a consequence of the inhomogeneity of the building materials our indoor environment is made of. Our model enables the analysis of a communication channel for both the narrow and wide band cases between adjacent rooms. We compare our analysis with real world measurements performed in our laboratory and obtain an adequate correspondence between our model results and the measurement. Our results indicate that the dielectric constant of the materials is frequency dependent.

Key-Words: - Communications, RF, Propagation Models

1 INTRODUCTION

During recent years, wireless communications have become an issue of extensive research. The Wireless Local Area Network (WLAN) is used to communicate between nodes up to few tens of mega bits per second. The conventional designated frequencies for WLAN systems are within the Industrial Scientific and Medical (ISM) 2.4-2.4835 band and the Unlicensed National Information Infrastructure (UNII) 5.15-5.35GHz and 5.725-5.825GHz bands.

The Wireless Personal Area Network (WPAN) system is designed to provide short-range, high-speed multi-media data services to terminals located in rooms or office spaces. Two continuous blocks of frequencies were allocated for indoor short-range networks, the band of 3.1-10GHz and 59-64 GHz one [1]. The unique capabilities of the ultra wideband (UWB) technique may promise reliable links between nodes located in different rooms. It was suggested to integrate the 5GHz and the 60 GHz bands to enable operation in indoor and outdoor environments [2].

One of the principal challenges in realizing high data rate, wireless communication links in indoor or indoor-outdoor scenarios are the phenomena arising during the propagation of electromagnetic waves inside a construction [3]-[4]. Development of a channel model for continuous RF frequencies in indoor environments is required for the analysis of indoor communications in an ultra wide band wireless network which includes a single transmitting and a single receiving antenna. The building blocks of such a model include single frequency propagation coefficients which are later integrated to obtain the wideband response. The model developed here is in the frequency domain and thus allows analyzing dispersive effects in transmission and reflection of ultra short pulses in UWB communications from building materials which the room is made of in accordance with their complex dielectric coefficients. Transmission of UWB signals is dominated by the frequency dependent dielectric properties of the materials and structures composing the propagation medium. It is well recognized that walls introduce attenuation. However dispersive effects are also expected due to their multi slab structure, creating a dielectric resonator.

In this paper we present a space-frequency model for narrowband and wideband links, considering the complex dielectric properties of the materials of the building walls. Based on the approach, a numerical

model will be developed enabling examination of the absorptive and dispersive effects on propagation of radio waves through the walls at the super- and extremely- high frequencies. For this purpose a library of material characteristics of various materials (concrete, reinforced concrete, plaster, wood, blocks, glass, stone and more) in the standard frequency domain for wireless networks was previously assembled. In this work we will describe a model taking into account transmission through multiple layers which are a consequence of the inhomogeneity of the building materials our indoor environment is made of. Examples include hollow brick and plaster walls. Our model enables the analysis of a communication channel for both the narrow and wide band cases between adjacent rooms. Further more we compare our analysis with real world measurements performed in our laboratory and obtain a remarkable correspondence between our single frequency theoretical results and the measurement results in a large range of frequencies. Despite the similarities our results indicate that the dielectric constant is frequency dependent.

To conclude, in addition to the new concise formulation of a narrow and wide band propagation model through multi-layer structure. We also confront our model with experimental results. This distinguishes our works from other works which are pure theoretical and remote from real world applications:

Our results are relevant to real world materials and real world communication scenarios. Thus they differ from merely theoretical considerations which assume periodicity [17, 18, 19,20].

2 PRESENTATION OF ELECTROMAGNETIC WAVES IN THE FREQUENCY DOMAIN

The electromagnetic field in the time domain is described by the space-time electric $E(r,t)$ and magnetic $H(r,t)$ signal vectors. r stands for the $(\mathrm{x},\mathrm{y},\mathrm{z})$ coordinates, where (x,y) are the transverse coordinates and z is the axis of propagation. The Fourier transform of the electric field is defined by:

$$\mathbf{E}(r,f)=\int_{-\infty}^{+\infty}E(r,t)\cdot e^{-j2\pi ft}dt \qquad (1)$$

(Equations (1-6) are derived in reference [5]). Where f denotes the frequency. Similar expression is defined for the Fourier transform $\mathbf{H}(r,f)$ of the magnetic field. Since the electromagnetic signal is real (i.e. $E^{*}(r,t)=E(r,t)$), its Fourier transform satisfies $\mathbf{E}^{*}(r,f)=\mathbf{E}(r,-f)$. A complex representation of the signal is given by the expression [5]:

$$\tilde{E}(r,t)=E(r,t)+j\hat{E}(r,t) \qquad (2)$$

where

$$\hat{E}(r,t)=\frac{1}{\pi t}*E(r,t)=\int_{-\infty}^{+\infty}\frac{E(r,t')}{\pi(t-t')}dt' \qquad (3)$$

is the Hilbert transform of $E(r,t)$. Fourier transformation of the complex representation (2) results in a 'phasor-like' function $\tilde{\mathbf{E}}(r,f)$ defined in the positive frequency domain and related to the Fourier transform by:

$$\tilde{\mathbf{E}}(r,f)=\begin{cases}2\mathbf{E}(r,f) & f>0\\ 0 & f<0\end{cases} \qquad (4)$$

The Fourier transform can be decomposed in terms of the phasor like functions according to:

$$\mathbf{E}(r,f)=\frac{1}{2}\tilde{\mathbf{E}}(r,f)+\frac{1}{2}\tilde{\mathbf{E}}^{*}(r,-f) \qquad (5)$$

and the inverse Fourier transform is then:

$$E(r,t)=\int_{-\infty}^{+\infty}\mathbf{E}(r,f)\cdot e^{+j2\pi ft}df=\mathrm{Re}\int_{0}^{\infty}\tilde{\mathbf{E}}(r,f)\cdot e^{+j2\pi ft}df \qquad (6)$$

3 ELECTROMAGNETIC WAVES IN DIELECTRIC MEDIA

Propagation of electromagnetic waves in a medium can be viewed as a transformation through a linear system (see reference [6] for a complete derivation of equations (7-12)). A plane wave propagating in a (homogeneous) medium is given in the frequency domain by:

$$\tilde{\mathbf{E}}_{out}(f)=\tilde{\mathbf{E}}_{in}(f)\cdot e^{-jk(f)d} \qquad (7)$$

Here, $k(f)=2\pi f\sqrt{\mu\varepsilon}$ is a frequency dependent propagation factor, where ε and μ are the permittivity and the permeability of the material composing the medium, respectively. In a dielectric medium the permeability is equal to that of the vacuum $\mu=\mu_0$ and the permittivity is given by $\varepsilon(f)=\varepsilon_r(f)\cdot\varepsilon_0$. The polarization in dielectric materials with absorption is accounted via a complex relative permittivity:

$$\varepsilon_r(f)=\varepsilon'(f)-j\varepsilon''(f) \qquad (8)$$

The relative permittivity is a frequency dependent quantity with a real part $\varepsilon'(f) \geq 1$ and an imaginary part $\varepsilon''(f)$. The ratio between the imaginary and real parts is known as the 'loss tangent' $tg[\delta(f)] = \frac{\varepsilon''(f)}{\varepsilon'(f)}$.

The propagation factor can be presented by:

$$k(f) = \frac{2\pi f}{c}\sqrt{\varepsilon_r(f)} = \frac{2\pi f}{c/\sqrt{\varepsilon'(f)}} \cdot \sqrt{1 - j \cdot tg[\delta(f)]} \quad (9)$$

where $c = \frac{1}{\sqrt{\mu_0 \varepsilon_0}}$ is the speed of light. The propagating wave can be written as:

$$\mathbf{E}_{out}(f) = \mathbf{E}_{in}(f) \cdot e^{-[\alpha(f) + j\beta(f)]d} \quad (10)$$

where $\alpha(f) = -\mathrm{Im}\{k(f)\}$ is the attenuation coefficient and $\beta(f) = \mathrm{Re}\{k(f)\}$ is the wave number of the propagating wave. The real and imaginary parts are determined from:

$$\begin{aligned} \alpha^2(f) - \beta^2(f) &= -\left(\frac{2\pi f}{c}\right)^2 \varepsilon'(f) \\ 2\alpha(f)\beta(f) &= \left(\frac{2\pi f}{c}\right)^2 \varepsilon'(f) tg(\delta) \end{aligned} \quad (11)$$

Solution of the set (11) results in [6]:

$$\begin{aligned} \alpha(f) &= \frac{2\pi f}{c}\sqrt{\frac{\varepsilon'(f)}{2}\left\{\sqrt{1 + tg^2[\delta(f)]} - 1\right\}} \\ \beta(f) &= \frac{2\pi f}{c}\sqrt{\frac{\varepsilon'(f)}{2}\left\{\sqrt{1 + tg^2[\delta(f)]} + 1\right\}} \end{aligned} \quad (12)$$

The dielectric properties of several building materials are summarized in Table 1 for frequencies of 5GHz.

4 WAVE PROPAGATION IN A DIELECTRIC LAYER

Consider a dielectric slab of thickness d, as illustrated in figure 1. The problem of transmission and reflection of an incident wave can be treated as done for a Fabry-Perot etalon [7]-[8].

When the wave is incident at an angle θ relative to the normal of the interface between dissimilar media, the field reflection coefficient is given by [9]:

$$\begin{aligned} r &= \rho_0\left\{1 - \left[\left(1 - \rho_0^2\right)e^{-j2k_z(f)d}\right]\sum_{i=0}^{\infty}\left[\rho_0^2 e^{-j2k_z(f)d}\right]^i\right\} = \\ &= \rho_0 \cdot \frac{1 - e^{-j2k_z(f)d}}{1 - \rho_0^2 e^{-j2k_z(f)d}} = \rho_0 \cdot \frac{1 - e^{-2(\alpha + j\beta)\cos(\theta)d}}{1 - \rho_0^2 e^{-2(\alpha + j\beta)\cos(\theta)d}} \end{aligned} \quad (13)$$

The coefficient ρ_0 is resulted from the Fresnel's equations [9]-[10] (equations (13-19) are derived in references [9,10]). When the electric field component of the wave is perpendicular to the plane of incidence (TE-wave):

$$\rho_{0-TE} = \frac{\cos(\theta_0) - \sqrt{\varepsilon_r - \sin^2(\theta_0)}}{\cos(\theta_0) + \sqrt{\varepsilon_r - \sin^2(\theta_0)}} \quad (14)$$

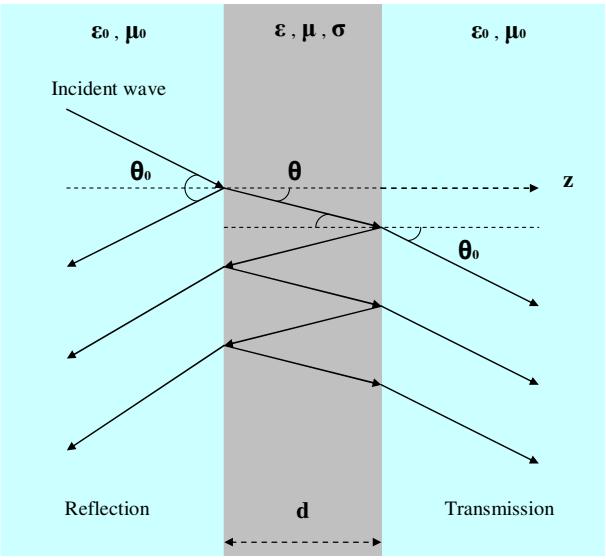

Fig. 1. Wave propagation in a dielectric slab.

For the case of parallel polarization, where the incident electric field vector is in the plane of incidence (TM-wave):

$$\rho_{0-TM} = \frac{\sqrt{\varepsilon_r - \sin^2(\theta_0)} - \varepsilon_r \cos(\theta_0)}{\sqrt{\varepsilon_r - \sin^2(\theta_0)} + \varepsilon_r \cos(\theta_0)} \quad (15)$$

The field transmission of the electromagnetic wave through the slab is described by the expression:

$$t = \frac{\left(1 - \rho_0^2\right)e^{-jk_z(f)d}}{1 - \rho_0^2 e^{-j2k_z(f)d}} = \frac{\left(1 - \rho_0^2\right)e^{-(\alpha + j\beta)\cos(\theta)d}}{1 - \rho_0^2 e^{-2(\alpha + j\beta)\cos(\theta)d}} \quad (16)$$

Transmission, reflection and loss of a single layer are depicted in figure 2.

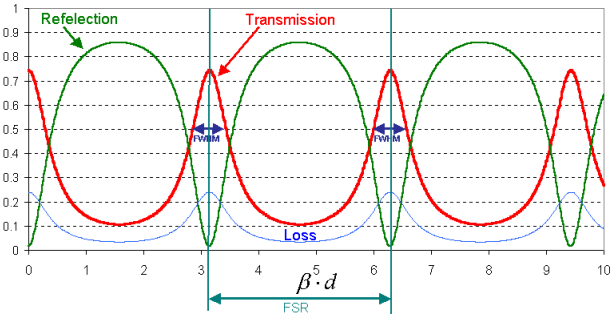

Fig. 2. Reflection, Transmission and Loss in a dielectric slab.

The free spectral range (FSR) between transmission peaks is given for low loss materials (small imaginary dielectric constant) by:

$$FSR \cong \frac{c}{2d \cdot \sqrt{\varepsilon'(f)} \cdot \cos(\theta)} \cdot \left[1 + \frac{f}{2\varepsilon'(f)} \cdot \frac{d\varepsilon'(f)}{df} \right]^{-1} \quad (17)$$

The full width at half maximum (FWHM) of the transmission peaks is given by:

$$FWHM = \frac{FSR}{Finesse} \quad (18)$$

In which the Finesse is defined by:

$$Finesse = \frac{\pi \sqrt{|\rho_0| e^{-\alpha \cos(\theta) d}}}{1 - |\rho_0| e^{-\alpha \cos(\theta) d}} \quad (19)$$

A realistic calculation for a concrete layer transmission and reflection coefficients is given in figure 3 and 4. The dielectric constants are taken from Table 1.

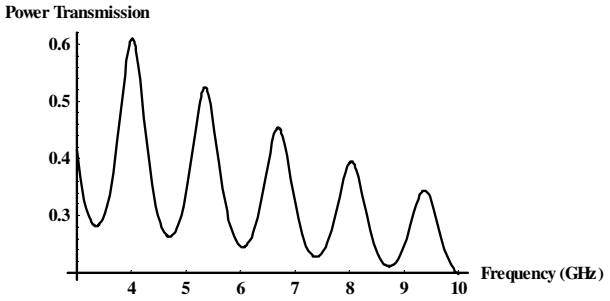

Fig. 3. Transmission coefficient of a one year d=5 cm concrete dielectric slab with TE polarization and 45 degrees to the normal.

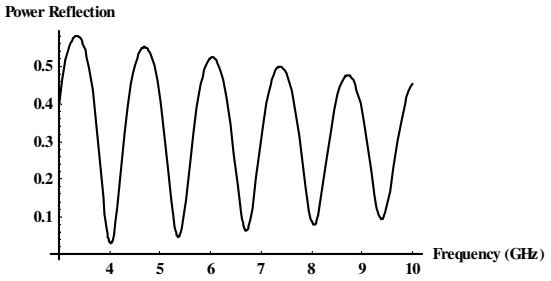

Fig. 4. Reflection coefficient of a one year d=5 cm concrete dielectric slab with TE polarization and 45 degrees to the normal.

TABLE 1
DIELECTRIC PROPERTIES OF BUILDING MATERIALS MEASURED AT 5 GHZ

MATERIALS	Relative Permittivity	
	Real	Imaginary
	ε'	ε"
Brick (made of chalk, with hole)	4.12	0.16
Brick (without hole)	3.3	0.01
Brick wall	3.56	0.34
Concrete (one year)	5.5	0.18
Concrete (40 years)	4.6	0.24
Wood (a)	2.05	0.296
Wood (b)	1.65	0.235
Plasterboard	2.02	0.05328
Chipboard	2.88	0.4879
Glass	5.98	1.0764

The same calculation for transmission and reflection coefficients of an air layer embedded between two concrete media is depicted in figure 5 and 6.

5 WAVE PROPAGATION IN MULTIPLE LAYERS

Consider the case in which two layers are involved, the situation is depicted in figure 7. In this case in addition to the internal reflections which occur in each single layer and are taken into account in equations (13) and (16) there are multiple reflections from one layer to another.

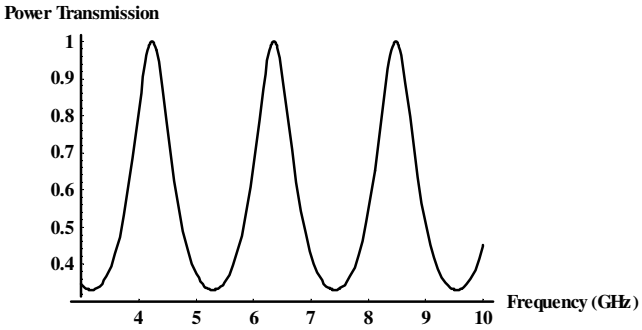

Fig. 5. Transmission coefficient of d=10 cm air layer in concrete medium with TE polarization and 45 degrees to the normal.

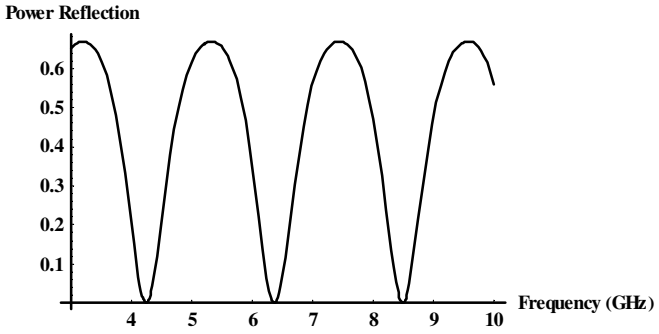

Fig. 6. Reflection coefficient of d=10 cm air layer in concrete medium with TE polarization and 45 degrees to the normal.

In this case we consider each layer as a lumped structure whose transmission and reflection coefficients t and r are given by equations (13) and (16) respectively. The coefficients of the first layer are denoted by t_1 and r_1 while coefficients of the second layer are denoted by t_2 and r_2. Summing up the reflection coefficients we arrive at reflection and transmission coefficients for the entire structure:

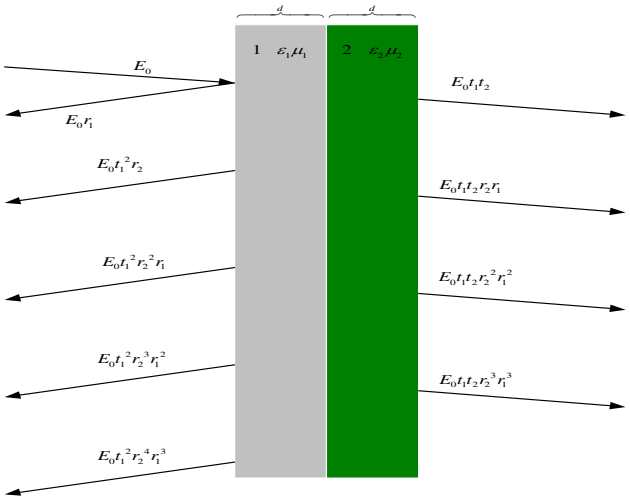

Fig. 7. Multiple reflections in a double slab structure.

$$t_{12} = t_1 t_2\left(1 + r_1 r_2 + (r_1 r_2)^2 + ...\right) = \frac{t_1 t_2}{1 - r_1 r_2} \qquad (20)$$

$$r_{12} = r_1 + t_1^2 r_2\left(1 + r_1 r_2 + (r_1 r_2)^2 + ...\right) = r_1 + \frac{t_1^2 r_2}{1 - r_1 r_2} \qquad (21)$$

This reasoning can be applied to a structure of three slabs depicted in figure 8.

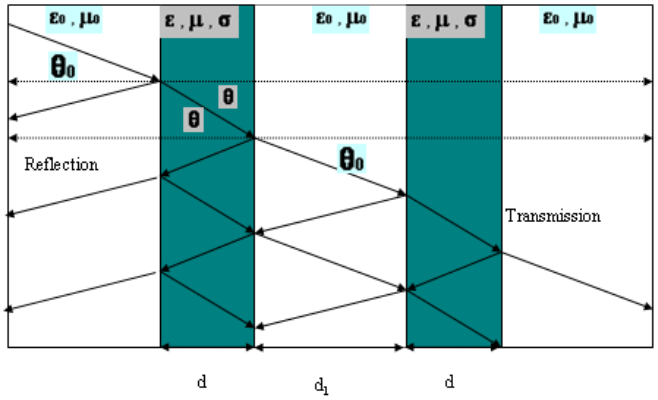

Fig. 8. Multiple reflections in a triple slab structure.

In this case the first two layers are considered as a lumped structure with reflection and transmission coefficients t_{12} and r_{12} respectively. Multiple reflections are now calculated between this lumped structure and the third layer. The three layer structure thus has the following transmission and reflection coefficients:

$$t_{123} = t_{12} t_3\left(1 + r_{12} r_3 + (r_{12} r_3)^2 + ...\right) = \frac{t_{12} t_3}{1 - r_{12} r_3} \qquad (22)$$

$$r_{123} = r_{12} + t_{12}^2 r_3\left(1 + r_{12} r_3 + (r_{12} r_3)^2 + ...\right) = r_{12} + \frac{t_{12}^2 r_3}{1 - r_{12} r_3} \qquad (23)$$

The same procedure can be generalized such that if the transmission and reflection coefficients of the n-1 layer structure are known to be $t_{Total(n-1)}$ and $r_{Total(n-1)}$ respectively then one can calculate the transmission and reflection coefficients of the n layer structure as follows:

$$t_{Total(n)} = t_{Total(n-1)} \cdot t_n\left(1 + r_{Total(n-1)} r_n + \left(r_{Total(n-1)} r_n\right)^2 + ...\right) = \frac{t_{Total(n-1)} t_n}{1 - r_{Total(n-1)} r_n} \qquad (24)$$

$$r_{Total(n)} = r_{Total(n-1)} + t_{Total(n-1)}^2 r_n\left(1 + r_{Total(n-1)} r_n + ...\right) = r_{Total(n-1)} + \frac{t_{Total(n-1)}^2 r_n}{1 - r_{Total(n-1)} r_n} \qquad (25)$$

The reader should take care, however, that since the basic single layer coefficients are defined through boundary reflection coefficients that in

turn depend on the dielectric constants of the medium on the left and right hand sides of the boundary, one should indeed take the correct dielectric constants. The power transmission and reflection coefficients are illustrated for a triple layer as follows we consider a concrete "brick" which is modeled by a 5 cm layer of concrete followed by a 10 cm layer of air which is followed by a 5 cm layer of concrete again. Furthermore, we assume that a plane electromagnetic wave approaches the "brick" such that its k vector is in 45^0 to the vector normal to the layer and the electric field is TE polarized. One can appreciate the complexity of the transmission and reflection coefficients by studying figures 9 and 10.

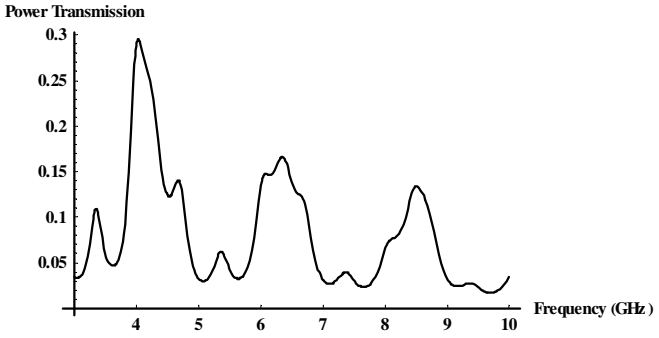

Fig. 9. Power transmission coefficient of a concrete brick. Air layer d=10 cm, Concrete layers d=5 cm each, TE polarization 45 degrees

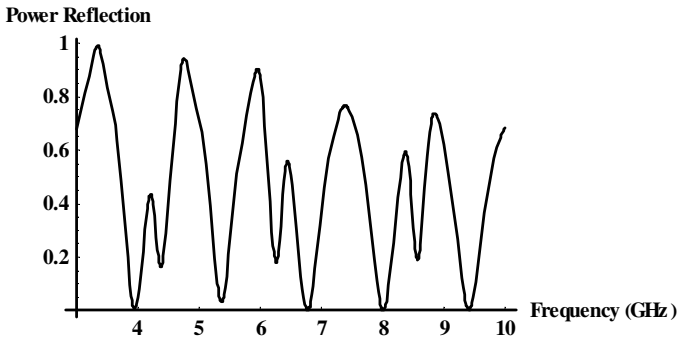

Fig. 10. Power reflection coefficient of a concrete brick. Air layer d=10 cm, Concrete layers d=5 cm each, TE polarization 45 degrees

6 EXPERIMENTAL RESULTS FOR SINGLE FREQUENCIES

In order to verify our transmission and reflection model we have used an Agilent 8757D Scalar network analyzer and an Agilent 83623B Swept signal generator. This device is in turn connected to HP 85025A signal detectors. In order to compare the power detected to the power transmitted a directive coupler is used. The same device is used in order to distinguish between injected and reflected signals in which both arrive at the same antenna. A Narde broadband high directive coupler 1-18 GHz Model 3292-2 is used. The antenna we use to transmit and receive the electromagnetic signals is a directional horn antenna of type JXTXLB-10180. Finally the entire measurement setup scheme for measuring both reflection and transmission coefficients is described in figure 11. In order to subtract the transfer function of the antennas themselves from the measured data one first calibrates the measurements using a void setup in which nothing is replaced between the antennas, this situation is depicted in figure 12. In this case the antenna transfer function is calculated according to equation (26):

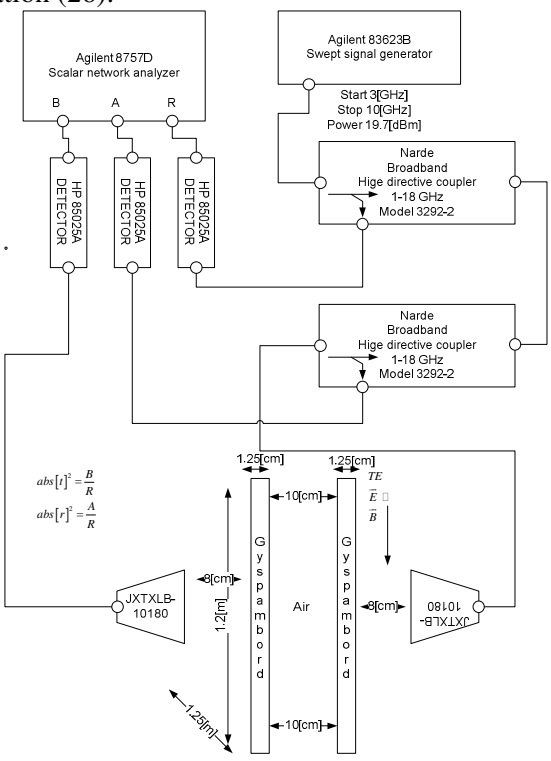

Fig. 11. Setup scheme for measuring both reflection and transmission coefficients

$$\frac{B_{antenna}}{R} = | H_{antenna} |^2 \quad (26)$$

Inserting an obstacle between the antennas we arrive by measurement at the transfer function:

$$\frac{B_{antenna+obstacle}}{R} = | H_{antenna+obstacle} |^2 \quad (27)$$

Those two measurements can be factorized to obtain the absolute square transfer function:

$$| t |^2 = \frac{| H_{antenna+obstacle} |^2}{| H_{antenna} |^2} \quad (28)$$

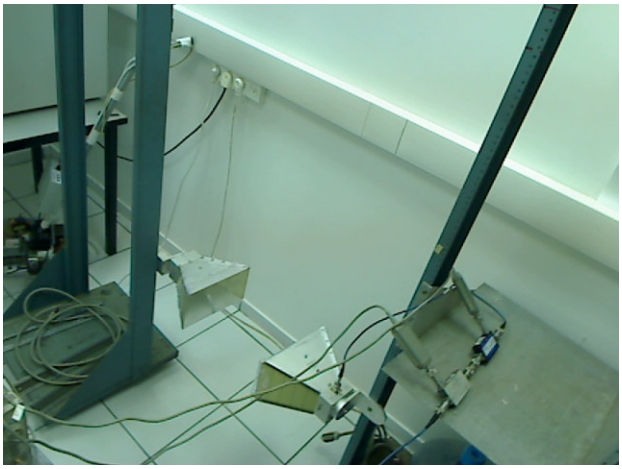

Fig. 12. Setup calibration for transmission.

Fig. 13. Measurement of a triple layer gypsum wall. The gypsum layers are d=10 cm apart the k vector angle with respect to the normal is 0^0.

Using the procedure described above we have measured the transmission coefficient through a triple layer gypsum wall as described in figure 13 below. The gypsum triple layer is made of two gypsum boards described in figure 14 and a 10 cm air gap in between. The results of measurement and comparison to the theory (which was previously developed) are given in figures 15 and 16 for 0^0 inclination. The same experiment is repeated for the case that the antennas are 45^0 to the wall normal and the results are depicted in figures 17 and 18. Although there is an apparent similarity between the theoretical and experimental curves they are not the same. The similarity is most apparent around the frequency of 5 GHz for which the dielectric constant is known through table 1 and was used to calculate the curve in the entire frequency range. Obviously this dielectric constant is frequency dependent and can not be considered to have the same value over the entire frequency range.

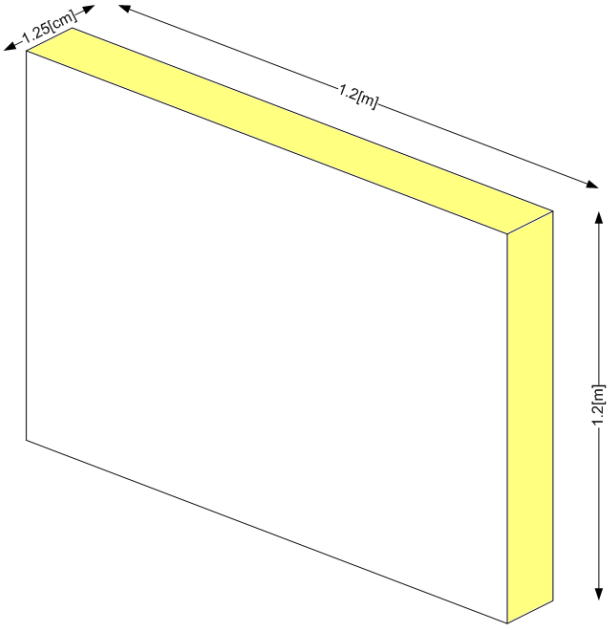

Fig. 14. Dimensions of the gypsum block used in our experiment.

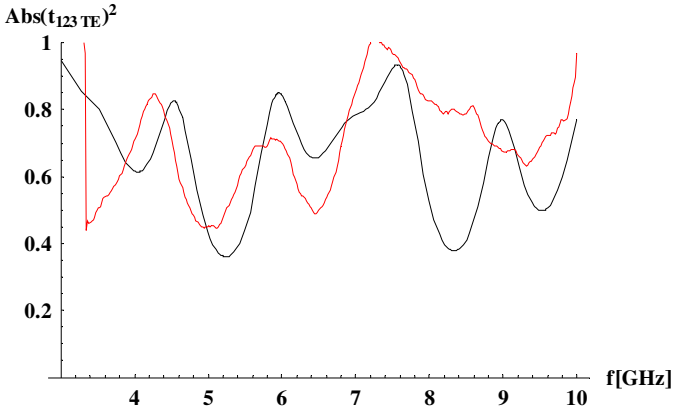

Fig. 15. Power transmission of the structure described in figure 13. The black curve describes theoretical predictions and the red curve measurement results.

Another system that we studied is a concrete wall depicted in figure 19. The wall is made of blocks whose geometrical dimensions are given in figure 20. Results of the measurements compared to the theory described previously are given for power transmission and reflection coefficients in figure 21 and 22 respectively. Those results appear to be worst than the one obtained for the gypsum wall although the theoretical and experimental curves still share some pronounced common features. This can be understood through the geometrical structure of the concrete block (figure 19) which resembles only superficially the infinite plane structure used to construct the theoretical transmission and reflection formulae 22 and 23. Indeed the block has some three dimensional structure that was not taken into account in the present theory. Again frequencies close to the 5 GHz frequency range for which we have knowledge of the complex dielectric constant through table 1 appear to be better matched to the theoretical results. This can be easily understood since it was the 5 GHz complex dielectric constant that was used to calculate the theoretical curves. This suggests that the dielectric constant change with frequency and its frequency dependence can be obtained from such measurements as presented here.

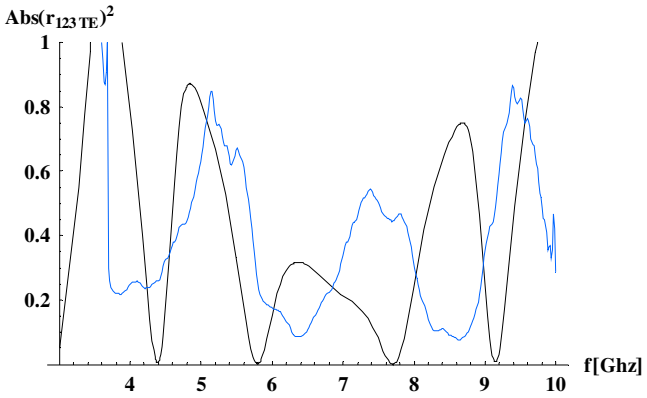

Fig. 16. Power reflection from the structure described in figure 13. The black curve describes theoretical predictions and the blue curve experimental results.

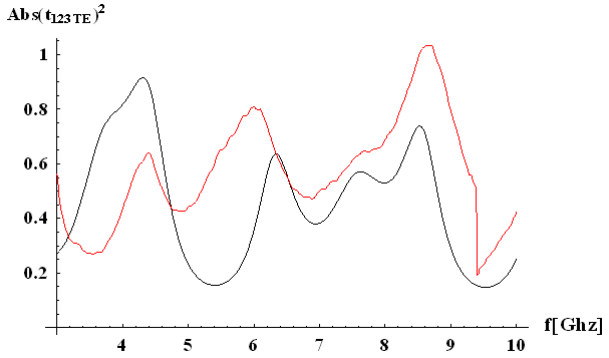

Fig. 17. Power transmission of the structure described in figure 13 but with 45^0 antenna inclination. The black curve describes theoretical predictions and the red curve measurement results.

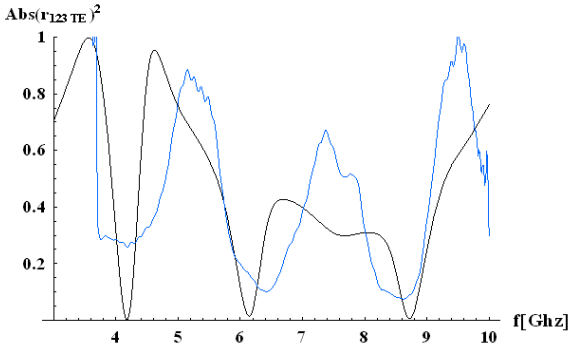

Fig. 18. Power reflection from the structure described in figure 13 but with 45^0 antenna inclination. The black curve describes theoretical predictions and the blue curve experimental results.

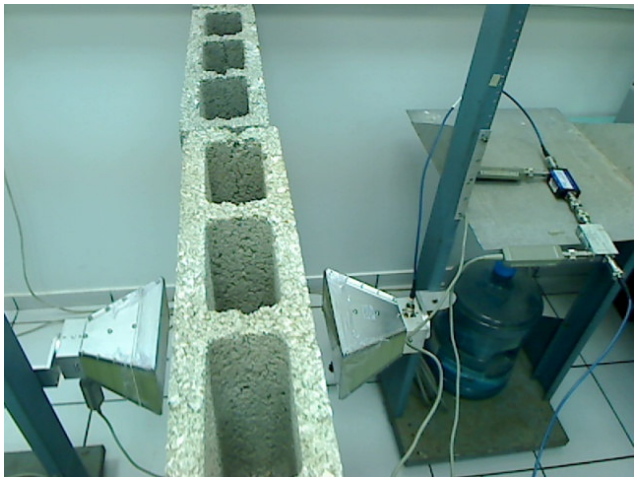

Fig. 19. Measurement of reflection and transmission from a concrete wall. The dimensions of each block in the wall are given in figure 20 below, the antennas are 8 cm from the wall and the k vector angle with respect to the normal is 0^0.

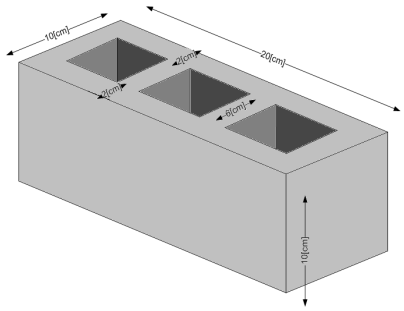

Fig. 20. Geometry of a concrete block used to construct the concrete wall depicted in figure 19.

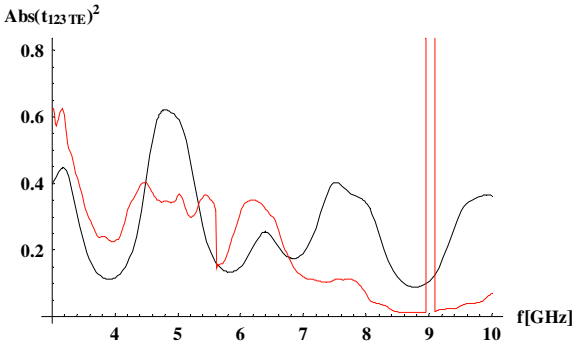

Fig. 21. Power transmission of the 10 cm thick concrete wall described in figure 19. The black curve describes theoretical predictions and the red curve measurement results. For unknown reason the detector saturated at about 9 GHz.

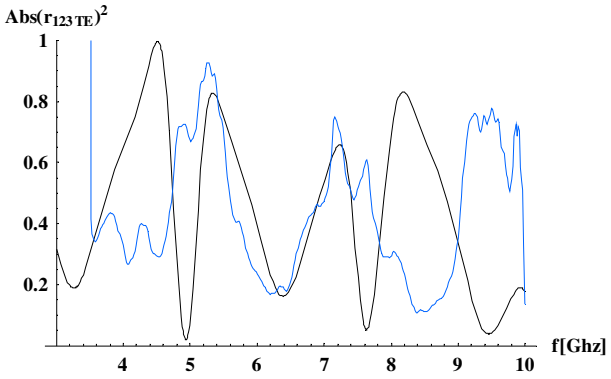

Fig. 22. Power reflection from a 10 cm thick concrete wall described in figure 19. The black curve describes theoretical predictions and the blue curve measurement results.

7 UWB PROPAGATION IN MULTIPLE LAYERS

The challenge of evaluating UWB transmission and reflection coefficients is tantamount to evaluating the transmission and reflection coefficients for each frequency component that the UWB pulse is made of and then integrating the results, this can be done as follows. Consider the wireless link depicted in figure 23. It was shown in [11] that given the channel modulated input signal to be:

$$E_{in}(t) = \mathrm{Re}\left\{A_{in}(t)\cdot e^{j2\pi f_0 t}\right\}. \tag{29}$$

And the channel modulated output signal to be:

$$E_{out}(t) = \mathrm{Re}\left\{A_{out}(t)\cdot e^{j2\pi f_0 t}\right\} \tag{30}$$

In which f_0 is the modulation frequency. The unmodulated output and input signals are related by:

$$A_{out}(t) = I_{out}(t) - jQ_{out}(t) = \\ = \int_{-\infty}^{+\infty} \mathbf{A}_{in}(f)\cdot H(f+f_0)\cdot e^{+j2\pi ft}\,df \tag{31}$$

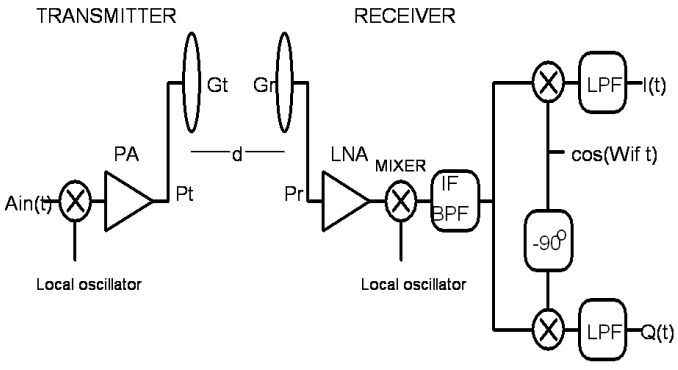

Fig. 23 Wireless link schematics.

The schematics for calculating the output pulse are given in figure 24:

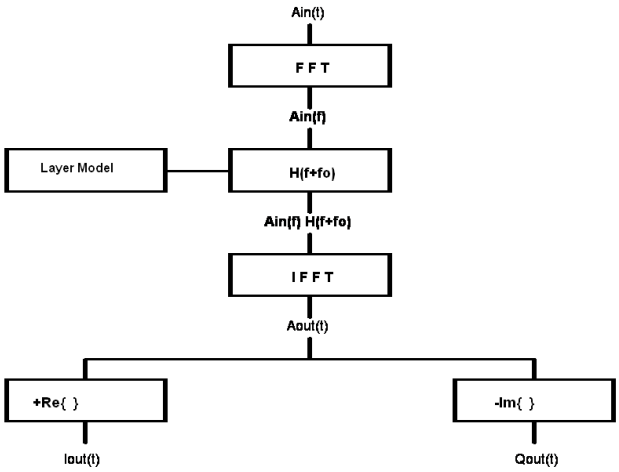

Fig. 24. Numerical integration scheme.

For reflected pulses the transfer function $H(f)$ is given by the single frequency reflection coefficient while for transmitted pulses the single frequency transmission coefficient serves the same purpose. Consider an input pulse of the form:

$$A_{in}(t) = e^{-\frac{t^2}{2\sigma_{in}{}^2}} \tag{32}$$

Assume that the pulse has a (standard deviation) width $\sigma_{in} = 0.1ns$, the pulse is depicted in figure 25. The Fourier transform of this pulse will also be a Gaussian given by:

$$\mathbf{A}_{in}(f) = \sqrt{2\pi}\cdot\sigma_{in}\cdot e^{-\frac{1}{2}(2\pi\sigma_{in}f)^2} \tag{33}$$

with a (standard deviation) width $\sigma_f = \frac{1}{2\pi\sigma_{in}} \cong 1.6GHz$, the normalized Fourier transform is described in figure 26.

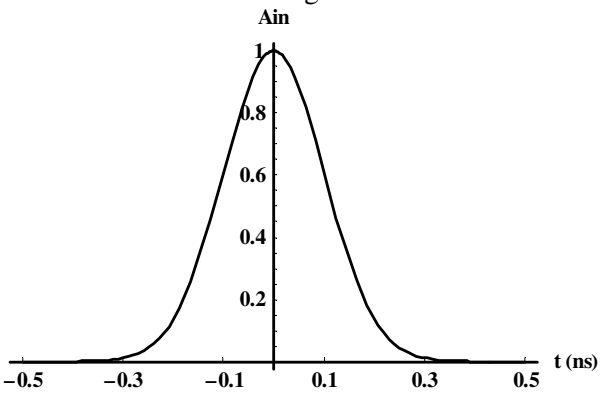

Fig. 25. A Gaussian pulse of standard deviation width of 0.1 ns.

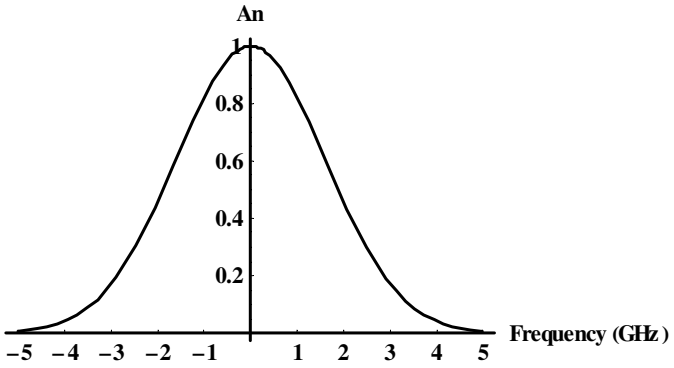

Fig. 26. The normalized Fourier transform of the Gaussian pulse of depicted in figure 25.

In what follows we consider a transmission of the pulse described above centered at $f_0 = 5GHz$ through a one year d=5 cm concrete dielectric slab with TE polarization and a k vector which is 45 degrees to the normal. The result calculated using the equations described above is given in figure 27.

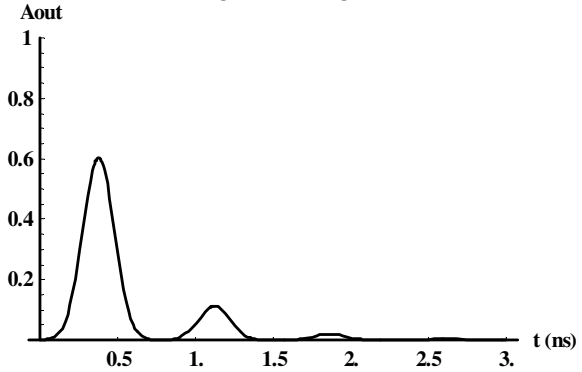

Fig. 27. Transmission of a Gaussian pulse through a one year d=5 cm concrete dielectric slab with TE polarization and 45 degrees to the normal.

It can be clearly seen the concrete slab introduces a delay and that the multiple reflections inside that slab create additional pulses with decreasing amplitude (due to absorption) of which the first two are discernible. The delay can be easily calculated by dividing the slab width d by the velocity of light in concrete v approximately:

$$\Delta t_{concrete} \cong \frac{d}{v} = \frac{d\sqrt{\varepsilon_r}}{c} \cong 0.39\,ns\,. \tag{34}$$

In the above c is the velocity of light in vacuum and ε_r is the relative dielectric constant of concrete given in table 1. Multiple reflections inside the slab also

affect the reflected pulse from the same slab calculated using previously described equations and depicted in figure 28. Notice that the first reflection has a zero time delay since the signal is assumed to be injected at zero distance from the concrete slab.

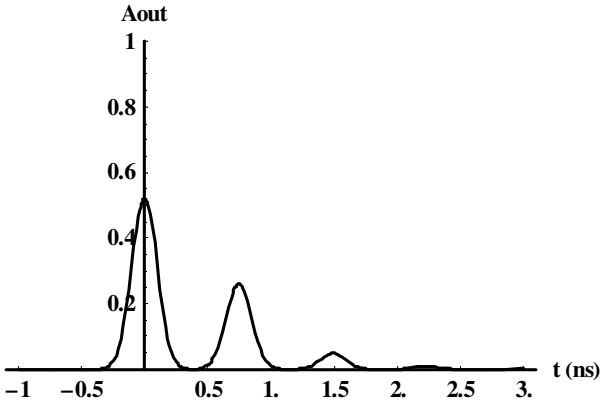

Fig. 28. Reflection of a Gaussian pulse from a one year d=5 cm concrete dielectric slab with TE polarization and 45 degrees to the normal.

The same calculations are repeated for an air gap embedded in a concrete media. Figure 29 describes a transmitted Gaussian pulse through an air gap of d=10 cm with TE polarization and 45 degrees of the k vector to the normal. The calculation is performed using previously described equations.

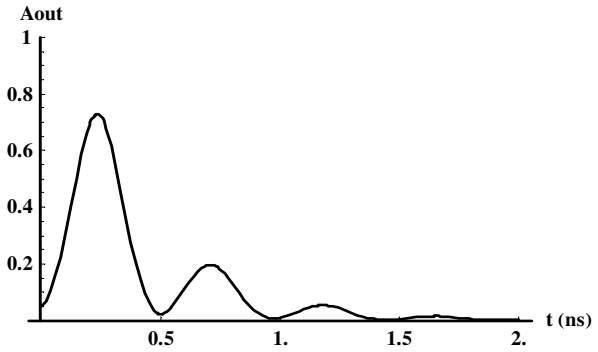

Fig. 29. Transmission of a Gaussian pulse through d=10 cm air gap in a one year concrete medium with TE polarization and 45 degrees to the normal.

Here the delay time is simply:

$$\Delta t_{air\ gap} \cong \frac{d}{c} \cong 0.33\,ns\,. \qquad (35)$$

Again multiple reflections can be easily seen. For reflections we calculate the graph depicted in figure 30:

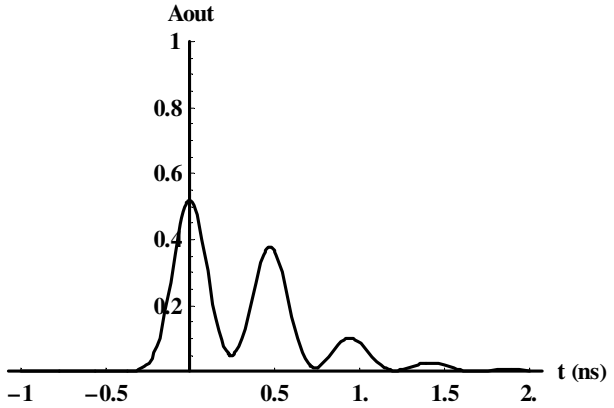

Fig. 30. Reflection of a Gaussian pulse from a d=10 cm air gap in a one year concrete medium with TE polarization and 45 degrees to the normal.

Finally we can combine the results for concrete slabs and air gap through the transmission and reflection formulae and equation (31) to calculate the transmission and reflection of a UWB short pulse through a concrete "brick" model. The "brick" is modeled by a 5 cm layer of concrete followed by a 10 cm layer of air which is followed by a 5 cm layer of concrete again. Furthermore, we assume that a plane electromagnetic wave approaches the "brick" such that its k vector is in 45^0 to the vector normal to the layer and the electric field is TE polarized. The complex resulting transmitted and reflected pulses is described in figures 31 and 32 respectively.

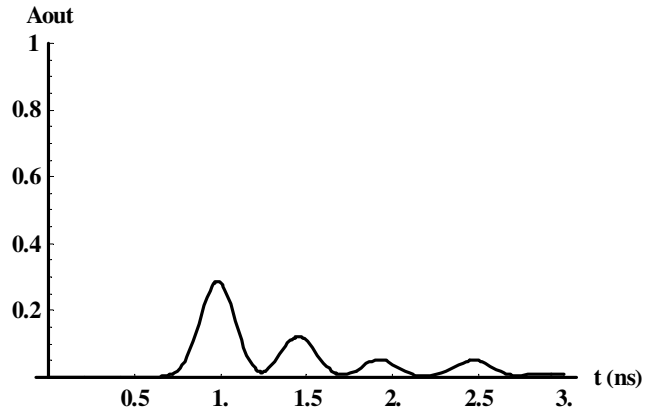

Fig. 31. A transmission of a Gaussian pulse through concrete brick. Air layer d=10 cm, Concrete layers d=5 cm each, TE polarization 45 degrees

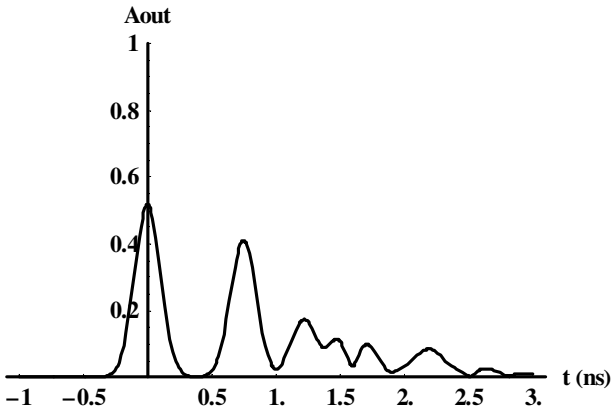

Fig. 32. A reflection of a Gaussian pulse from a concrete brick. Air gap is d=10 cm, Concrete layers d=5 cm each, TE polarization 45 degrees

As expected multiple reflections inside the brick result in a complex structure of reflected and transmitted pulses which in some cases overlap each other. This may have a profound effect on UWB communications in which reflections from early signals may appear as "noise" for later signals. The time delay of the first transmitted signal is:

$$\Delta t_{brick} \cong 2 \cdot \Delta t_{concrete} + \Delta t_{air\ gap} \cong 1.1\ ns \quad (36)$$

The time delay for the second reflected signal is:

$$\Delta t_{\mathrm{sec}ond\ \ reflection} \cong 2 \cdot \Delta t_{concrete} \cong 0.78\ ns \quad (37)$$

8 CONCLUSION

A theory for multi layer transmission and reflection was developed for narrow band (single frequency) and wide band (UWB=short temporal pulse) communications. The narrow band results were compared to experiment. Many other experiments which were not reported here due to lack of space will be reported elsewhere. Although the experiment and theory show considerable similarity there are improvements to be made in both experiment and theory. From the experimental point of view one should perform the experiment in a "reflection free" room and in a "far field" distance from the antenna those more accurate experiments are planned for the near future. From the theoretical point of view the frequency dependence of the dielectric constant should be taken into account. We hope that better understanding of channel properties in indoor environment will be helpful in designing "smart homes" and in fact in any indoor wireless application such as robot control [13], sensor network [14], wireless power meter communications [15] and interactive wireless whiteboard technology [16].

9 ACKNOWLEDGEMENT

The authors wish to acknowledge the assistance and support of the Israeli Short Range Consortium (ISRC) which is partially financed by the Israeli ministry of industry and commerce.

References:

[1] P. Smulder: “Exploiting the 60GHz Band for local wireless multimedia access: prospects and future directions.” IEEE *Communication Magazine*, pp. 140-147, January 2002.

[2] IST-BROADWAY WP1-D2 deliverable: “Functional system parameters description”, (October 2002)

[3] T. S. Rappaport, S. Sandhu: “Radio-wave propagation for emerging wireless personal communication systems”, IEEE *Antenna an Propagation Magazine,* vol. 36, pp. 14-36. 1994.

[4] A. Safaai-Jazi, S. M. Riad, A. Muqaubel, A. Bayram: “Report on through –the-wall propagation and material characterization”, carried out in the framework of the DARPA NETEX program “Ultra-wideband propagation measurements and channel modeling”, (November 2002)

[5] Y. Pinhasi, Yu. Lurie, A. Yahalom: “Space-frequency model of ultra wide-band interactions in millimeter wave masers”, Phys. Rev. E 71, 036503, 2005.

[6] P. Diament, *Wave transmission and fiber optics*, Maxwell Macmillan International Editions, 1990.

[7] C. Fabry, A. Perot: “Theorie et applications d’une nouvelle methode de spectroscopie interferentielle”, Ann. Chim. Phys., vol. 16, pp. 115, 1899.

[8] A. Yariv, *Quantum Electronics*, Wiley, 1988.

[9] H. J. Reed, T. S. Rappaport, B. D. Woerner, *Wireless Personal Communications: Advances in Coverage and Capacity*, Kluwer Academic Publishers , 1997.

[10] A. H. Cherin, *An Introduction to optical fibers*, McGraw Hill, 1985.

[11] Y. Pinhasi, A. Yahalom, O. Harpaz & G. Vilner “Study of an Ultra Wideband Transmission in the Extremely High Frequency (EHF) Band” IEEE Transactions on Antennas and Propagation Vol. 52, No. 11, 2833-2842, 2004.

[12] A. Yahalom, Y. Pinhasi, E. Shifman and S. Petnev "Transmission through Multiple Layers in UWB and Narrow Band Communications" proceedings of the COMCAS 2009 conference.

[13] A. Ali, M. Fezari, A. Hamza "High Level Tele-Operating Speech Communication System for Controlling a Colony of Robots" WSEAS Transactions on Communications Issue 6, Volume 9, 2010.

[14] R. S. J. Reyes, J. Claro Monje, M. Ericson, C. Santos, L. A. Mateo, R. Lynne, G. Espiritu, J. Isiderio, C. Miguel, M. Lacson, R. Edwin, T. Ocfemia "Implementation of Zigbee-based and ISM-based Wireless Sensor and Actuator Network with Throughput, Power and Cost Comparisons" WSEAS Transactions on Communications Issue 7, Volume 9, 2010.

[15] P. Mlynek, M. Koutny and J. Misurec, "The Communication Unit of Measuring Device in Power Engineering" WSEAS Transactions on Communications Issue 1, Volume 8, 2009.

[16] C. Shen and H. Chuang, "An Investigation on User Communication Behavior in an Interactive Whiteboard Technology Environment" WSEAS Transactions on Communications Issue 1, Volume 8, 2009.

[17] D. Kokody, S. Prosvirnin, "Analysis of electromagnetic characteristics of multi-layered periodic structures with turning layers" Mathematical Methods in Electromagnetic Theory (MMET 2000), Volume 1, p. 256 – 258.

[18] David J. White, "Transmission of Monochromatic Electromagnetic Waves through Systems Consisting of Multiple Layers of Materials Exhibiting Birefringence or Faraday Rotation" Research summary rept., Naval Weapons Center China Lake Calif, March 1977.

[19] V. M. Fomin & E. P. Pokatilov, "Optical Properties of Multi-Layer Structures. II. Reflection and Transmission" Physica Status Solidi (b), Volume 136, Issue 2, pages 593–602, 1 August 1986.

[20] C. H. Gan & G. Gbur "Extraordinary optical transmission through multi-layered systems of corrugated metallic thin films" Optics Express, Vol. 17, No. 22, pages 20553- 20566, 2009.

Asher Yahalom is an Associate Professor in the Faculty of Engineering at the Ariel University Center of Samaria and the Academic director of the free electron laser user center which is located within the University Center campus. He was born in Israel on November 15, 1968, received the B.Sc., M.Sc. and Ph.D. degrees in mathematics and physics from the Hebrew University in Jerusalem, Israel in 1990, 1991 and 1996 respectively. Asher Yahalom was a postdoctoral fellow (1998) in the department of electrical engineering of Tel-Aviv University, Israel. In 1999 he joined the faculty of the Ariel University Center of Samaria. During the years 2005-2006 he was a Senior Academic Visitor in the University of Cambridge, Cambridge, UK. Details can be found in: http://www.ariel.ac.il/sites/ayahalom/

Elhanan Shifman was born in Israel on July 23, 1982. He received the degree in electrical engineering from The University Center of Judea and Samaria, Ariel, Israel in 2009. Now he works there toward his M.Sc. Degree. His work is aimed at research of Multipath of electromagnetic waves in close indoor environment. Elhanan also work as a FPGA and signal processing engineer in GPS applications in a start up company.

Sergey Petnev was born in Moscow, Russia on 9 Sep. 1972. He received a B. Tech degree in electrical and electronic engineering from the University Center of Samaria, Ariel, Israel, in 2005. In the same year he joined the Israeli Short Range Consortium (ISRC) and has been engaged in the research of the indoor propagation of ultra wide band signals for wireless communications. He is currently employed in private company and studying for M.Sc. Degree in electronics engineering.

Yosef Pinhasi is the Dean of the Faculty of Engineering at the Ariel University of Samaria. He was born in Israel on May 3, 1961, received the B.Sc., M.Sc. and Ph.D. degrees in electrical engineering from Tel-Aviv University, Israel in 1983, 1989 and 1995 respectively. He served as the head of the Department of Electrical and Electronic Engineering between the years 2004-2007.

Since 1990 he is working in the field of electromagnetic radiation, investigating mechanisms of its excitation and generation in high power radiation sources like microwave and millimeter wave electron devices, free-electron lasers (FELs) and masers. He developed a unified coupled-mode theory of electromagnetic field excitation and propagation in the frequency domain, enabling study of wideband interactions of electromagnetic waves in media in the linear and non-linear (saturation) operation regimes.

Prof. Pinhasi investigates utilization of electromagnetic waves in a wide range of frequencies for various applications such as communications, remote sensing and imaging. The space-frequency approach, which developed by him, is employed to study propagation of wide-band signals in absorptive and dispersive media in broadband communication links, and wireless indoor and outdoor networks as well as in remote sensing Radars operating in the millimeter and Tera-Hertz regimes.